ADVANCED FUNCTIONAL MATERIALS

Supporting Information

for *Adv. Funct. Mater.*, DOI: 10.1002/adfm.201809111

Role of Interface Chemistry in Opening New Radiative Pathways in InP/CdSe Giant Quantum Dots with Blinking-Suppressed Two-Color Emission

*Allison M. Dennis, Matthew R. Buck, Feng Wang, Nicolai F. Hartmann, Somak Majumder, Joanna L. Casson, John D. Watt, Stephen K. Doorn, Han Htoon, Milan Sykora, and Jennifer A. Hollingsworth**

Supporting Information

Role of Interface Chemistry in Opening New Radiative Pathways in InP/CdSe Giant Quantum Dots with Blinking-Suppressed Two-Color Emission

*Allison M. Dennis, Matthew R. Buck, Feng Wang, Nicolai F. Hartmann, Somak Majumder, Joanna Casson, Stephen K. Doorn, Han Htoon, Milan Sykora, and Jennifer A. Hollingsworth**

S1. Experimental Methods

S1.1. Nanocrystal Synthesis

*Materials***:** Indium(III) chloride ($InCl_3$, anhydrous, Sigma Aldrich), Indium (III) acetate (99.99%-In, puratrem, Strem Chemicals), tris(trimethyl silyl)phosphine ($(TMS)_3P$, 95% Strem Chemicals or 98% Sigma Aldrich), selenium (amorphous shot, 1-3 mm, 99.999%, Alfa Aesar), sulfur (powder, 99.999%, Acros Organics), trioctylphosphine oxide (TOPO, 99%, Acros), trioctylphosphine (TOP, 97%, Sigma Aldrich), oleylamine (technical grade, 70%, Sigma Aldrich or Acros Organics), dioctylamine (98%), 1-octadecene (ODE, technical grade 90%, Acros), *n*-octadecane (OD, 99%, Alfa Aesar), cadmium oxide, (CdO powder, 99.998%, Alfa Aesar), myristic acid (MA, 99.5+%, Acros Organics), and oleic acid (OA, 90%, Alfa Aesar) were used as received without any further purification. All solvents purchased were anhydrous and used as received. All syntheses and processing of stock solutions and nanocrystals (with the exception of photochemical InP etching using HF) were performed under Ar atmosphere using standard air-free Schlenk techniques.

*Preparation of stock solutions***:** A 0.2 M cadmium oleate solution ($Cd(OA)_2$; 1:4 or 1:10 Cd:OA molar ratio) was prepared by stirring CdO in a mixture of OA and ODE under vacuum while heating to 100 °C before heating to at 260 °C under argon, followed by vacuum removal of water at 80°C. Stock solutions of TOP-Se (1.0 M) were prepared by stirring Se in TOP for several hours on a hot plate warmed to 70 °C under air-free conditions. Sulfur solutions were typically 0.2 M, and were prepared by dissolving sulfur powder in either ODE or OD at 180°C. A 0.2 M solution of indium myristate (In:MA 1:4) was prepared by mixing

indium (III) acetate and myristic acid in ODE at 120°C under vacuum for several hours. A 0.1 M stock solutions of $(TMS)_3P$ were prepared in ODE as well as mixtures of OA:ODE and dioctylamine:ODE (3:4 v:v) in a glovebox.

Preparation of InP core QDs, Method 1: InP QDs were synthesized using two distinct protocols, one using indium alkanoate as the indium precursor and the other using an indium halide solubilized with a phosphine oxide. The size series presented in Figures 1 and 2, the 1.8 nm, 1.9 nm, and 2.4 nm diameter InP cores were synthesized using Method 1. 5 mL of the indium myristate stock solution was heated to 188 °C in a 100 mL round-bottomed flask outfitted with a condenser. Several syringes containing $(TMS)_3P$ stock solution were removed from the glovebox and added to the indium myristate solution as follows: for the 1.8 nm cores, a 1.5 mL bolus of 0.1 M $(TMS)_3P$ in OA/ODE was injected and the temperature dropped to 178°C, where it was maintained. After 45 s, 1.5 mL of 0.1 M $(TMS)_3P$ in ODE was added to the solution dropwise over the span of 1 min, followed by a rapid reduction in temperature upon the injection of 20 mL of degassed ODE. The 1.9 nm diameter cores were produced similarly, but with an additional addition of 5 mL of the indium myristate stock solution followed by 3 mL of $(TMS)_3P$ in ODE added dropwise over 3 min at 178°C before quenching with ODE. To make the 2.4 nm cores, the addition of 5 mL In:MA and 3 mL $(TMS)_3P$ was repeated once more before the quenching with ODE. The 3.3 nm cores were produced similarly to the 1.8 nm core protocol described above, but with the dioctylamine $(TMS)_3P$ precursor rather than oleylamine; this reaction proceeded at 178 °C for 1 hour.

Preparation of InP core QDs, Method 2: Other InP QDs were synthesized, purified, and subjected to size-selective separation using published procedures.[1] Briefly, 0.350 g of anhydrous $InCl_3$, 10 mL TOP and 1 g TOPO were mixed under air-free conditions, and heated under Ar for 16 h at 100 °C. Enough $(TMS)_3P$ to satisfy a 1:1 In:P ratio was diluted slightly in hexane (to allow ease of handling by syringe), and injected at 100°C. After 3 h of heating at 100 °C, during which time the color progressed from colorless to yellow to orange to red, the temperature was ramped slowly to 260 °C and then the contents allowed to react for 3 days.

After cooling, the dark brown colloidal solution was purified by size-selective precipitation and centrifugation using toluene/methanol as solvent/non-solvent in an Ar-filled glovebox. Each purified nanocrystal fraction was stored in 3-5 mL of hexane. The InP core size and concentration was calculated from the 1S peak in the absorption spectrum, as described in the literature.[2]

Preparation of InP/CdSe and InP/CdSe/CdSe core/shell QDs: Successive ionic layer adsorption and reaction (SILAR) was used to grow CdSe and CdS shells on InP core nanocrystals in an iterative, monolayer-by monolayer process that was adapted from the shell growth method used to prepare InP/CdS core/shell gQDs.[3] For InP cores prepared using method 1, 2.0 $x10^{-7}$ mol cores suspended in hexanes were mixed with 1 mL oleylamine and 9 mL ODE. Hexanes were evaporated under vacuum at 80 °C, and the temperature was raised to 150 °C for addition of the first monolayer of CdSe. For subsequent monolayer additions, the reaction was held at 240 °C. For InP cores prepared using method 2, 1.0 $x10^{-7}$ mol of purified, size-selected InP cores in hexanes were mixed with 5 mL oleylamine and 4 mL ODE. Hexanes were evaporated as above, and the temperature was raised to 240 °C for SILAR shell addition. In both cases, alternating injections of 0.2 M Cd-oleate and either 0.2 M TOP-Se or 0.2 M sulfur in ODE were performed in a dropwise fashion, allowing 2-3 h of solution-phase annealing after each Cd-oleate addition and 1 h after each S addition. The delivered precursor volumes were calculated to yield one ML of CdS(e) shell per addition cycle.

Photochemical etching of InP cores using HF: Purified, size-selected fractions containing 1.0 x 10^{-7} mol InP nanocrystals were subjected to photochemical HF etching before shell growth. Photochemical etching was performed by adapting a published procedure with modification.[4] Specifically, InP cores were dissolved in 12-13 mL *n*-butanol containing 125 mg TOPO, and approximately 8 *u*L HF was added. A 150 W tungsten halogen lamp was used to illuminate the stirring samples from above in a wide-mouthed polyethylene bottle. The suspension was

irradiated overnight (16 h). QDs were precipitated using acetonitrile, collected using centrifugation, and then dispersed in hexanes.

Synthesis discussion. In all cases, reagents were stored and handled in an Ar-filled glovebox, and all synthetic and work-up procedures were performed using standard air-free Schlenk techniques. Various procedures were attempted to avoid exposing the InP cores to air prior to CdSe shell growth. These ranged from using sparged or freeze-vac degassed solvents and Ar-filled conical tubes capped with septa for core workup to conducting shell growth in the core growth solution ("one-pot reaction," i.e., no core workup) or restricting core workup to an Ar glovebox. An additional possible source of unintentional oxygen exposure, beyond the chosen core workup procedure, is the In precursor itself. Indium(III)acetate often contains trace water, which is known to hydrolyze the phosphine precursor and/or the nanocrystal surface, leading to accidental oxygen incorporation. For our core preparations, we both adapted a reaction between $InCl_3$ and tris(trimethylsilylphosphine) in TOPO(99%)/TOP(97%) solvent mixture, and used In(III) myristate generated from In(III) acetate in ODE. This difference in core synthesis can account for some of the variability we observed between reactions that were otherwise conducted in an equally air-free manner.

S1.2. Spectroscopy

Ensemble Spectroscopy. Purified InP, InP/CdSe and InP/CdSe/CdS QD samples were dispersed in tetrachloroethylene (TCE) for ensemble spectroscopic measurements. Absorption spectra were collected on a Cary Varian 5000 UV-Vis-NIR spectrophotometer, and two PL spectra were collected for each nanocrystal sample on a Horiba Yobin Jvon NanoLog spectrofluorometer using a 450 W Xe arc lamp for excitation. The first PL spectrum was collected on a R928 PMT covering the approximate range from 400-950 nm (for visible PL), and the second on a liquid N_2-cooled InGaAs CCD from approximately 800-1200 nm (NIR PL). After all spectra were corrected for detector inefficiency, the visible PL intensities were multiplied by a scaling factor that allowed the two spectra taken for each nanocrystal sample

to overlap, permitting the spectral intensities to be plotted across the entire wavelength range where dual emission was observed. Integration times ranged from 1-40 s.

Single-nanocrystal optical characterization. To perform optical characterization of single QDs, a QD suspension was diluted to achieve a sparse distribution of single nanocrystals (~1 QD per 4 μm^2) upon dropcasting onto a glass coverslip. Hexane was used for dilution, and ultra-dilution was carried out immediately prior to dispersal of the suspension onto the substrate to minimize QD-QD aggregation. A pulsed laser with 405 nm wavelength and ~80 ps pulse width was used to excite the QDs. A simplified optical setup diagram is shown in Figure S10. By a reflection-angle tunable mirror (i.e., the computer-controlled scanning mirror), the 405 nm laser beam was directed into an objective lens (100×, 0.85 NA), and then was focused on the QD sample through the objective. Before entering the objective lens, the incident angle of the 405 nm laser beam could be tuned by the scanning mirror, allowing the focused beam on the sample to be shifted at will. In this way, samples were scanned to locate the emitting QDs within a certain area. Photoluminescence from single QDs was then collected by the same objective lens and directed to two APDs, forming a Hanbury-Brown-Twiss spectrometer.

Since the interrogated single QDs may possess two emission bands, one below 690 nm and one above 720 nm, a 680 nm short-pass (SP) filter and/or a 720 nm long-pass (LP) filter was installed in front of APD 1 (switchable filters 1). Similarly, SP and LP filters were also installed before APD 2 (switchable filters 2). With a different filter before the two APDs, a quick, simultaneous dual-channel scan could be conducted to identify the emissive spots that radiated strongly at both the short band and the long band. Focusing on these dual-emission spots, the filters could then be switched to the same bands, so that both APDs could receive photons from the same wavelength range, either 680 SP or 720 LP. By this means, PL-intensity time traces and 2nd order photon-correlation traces, or g(2) values, from these dual-band emission spots could be measured and analyzed for either the short-band or the long-band emission, the latter [g(2)] to confirm the single-QD nature of the observed spot.

Alternatively, leaving the different filters in front of each APD, a cross-correlation g(2) value could be obtained to determine whether or not the two emissions were correlated or if, instead, both colors are emitting in the same excitation cycle and are uncorrelated.

For far-field, dual-color images the microscope setup was slightly modified. A continuous wave laser at 405 nm was used for excitation and focused on the back-focal plane of the microscope objective to ensure wide-field excitation. A dichroic beam-splitter separates the QD emission from the excitation light and is focused through an interchangeable set of filters onto a TE cooled electron multiplying charge coupled device (EMCCD) camera. To subsequently record the two different emission channels a combination of a LP filter at 620 nm and a SP filter at 700 nm was used for the visible channel. A LP filter at 790 nm was used for the NIR channel. The two separate images were overlayed into a red and blue channel figure via ImageJ software.

TA spectroscopy. The TA spectra were recorded using a commercial pump–probe TA spectrometer (Helios, Ultrafast Systems). The femtosecond pump pulses at energy of 3.1 eV (400 nm) were generated by focusing a portion of the 800 nm output from 1 kHz regenerative amplifier (Spectra Physics) onto a BBO crystal. The probe pulse, a white light continuum, was generated by passing the second portion of the 800 nm output through a delay line and a 2mm sapphire crystal. The measured instrument response was 250 fs (FWHM). The diameter of the probe beam focused onto the sample was ~0.1 mm. The pump fluence was 6 mJ/pulse·cm^2, which corresponds to >20 photons absorbed by a QD, on average. Solutions were continuously stirred during the experiment to minimize the potential effects of photo-degradation and local heating.

Explanation of Mandel Q parameter and its relationship to assessing blinking suppressing. The Mandel Q parameter is defined as $Q = (\langle n^2 \rangle - \langle n \rangle^2)/\langle n \rangle$, where n represents the measured value of photoluminescence (PL) counts within the 100 ms time bin. It is known that a Poisson distribution can usually be used to express the probability distribution of the random occurrences of certain events in a fixed interval of time. In results reported here, the

Mandel Q parameter serves as an indicator of the variation in PL intensity distribution from the Poisson distribution for each PL time trace. For on-state quantum dots (QDs), the smaller the measured Mandel Q values, the smaller the PL variation is from a Poisson distribution. Usually, if Mandel Q values are smaller than 3, we can describe the PL blinking as having been effectively suppressed. In contrast, a large Q, i.e., >10, indicates poor suppression of PL blinking. According to the Mandel Q values shown in text Figure 4, both visible and infrared PL-blinking of core/shell QDs comprising InP/5CdSe/n-CdS are best suppressed when the CdS shell is sufficiently thick, namely, 7 monolayers of CdS. In this case, the proportion of QDs exhibiting Q<3 is the greatest and the proportion of QDs exhibiting Q>10 is the smallest, compared to QDs prepared using 1, 3, and 5 CdS monolayers.

PL intensity changes in response to elevated temperature. InP/5CdSe/4CdS and InP/5CdSe/7CdS were cycled between room temperature and 115 °C, where three main observations were made: (a) thicker CdS resulted in better recovery post-heating than thinner CdS (significantly so), (b) NIR PL recovers better than visible PL, (c) visible and NIR PL decrease approximately together for thinner CdS shells, but for thicker CdS, NIR decreases proportionally less than visible PL intensity, where latter results in opposite trends between NIR and visible in a plot of NIR-area/(NIR area+visible area) compared to visible-area/(NIR area+Vis area) [up vs. down]. Thus, thicker CdS affords better thermal stability for NIR PL compared to visible PL.

S1.3. References

[1] A. A. Guzelian, J. E. B. Katari, A. V. Kadavanich, U. Banin, K. Hamad, E. Juban, A. P. Alivisatos, R. H. Wolters, R.H., C. C. Arnold, J. R. Heath, *J. Phys. Chem.* **1996**, *100,* 7212.

[2] R. G. Xie, Z. Li, X. G. Peng, *J. Am. Chem. Soc.* **2009**, *131*, 15457.

[3] A. M. Dennis, B. Mangum, A. Piryatinski, Y.-S. Park, D. Hannah, J. Casson, D. Williams, R. Schaller, H. Htoon, J. A. Hollingsworth, *Nano Lett.* **2012**, *12*, 5545.

[4] D. V. Talapin, N. Gaponik, H. Borchert, A. L. Rogach, M. Haase, H. Weller, *J. Phys. Chem. B* **2002**, *106,* 12659.

S2. Supporting Figures

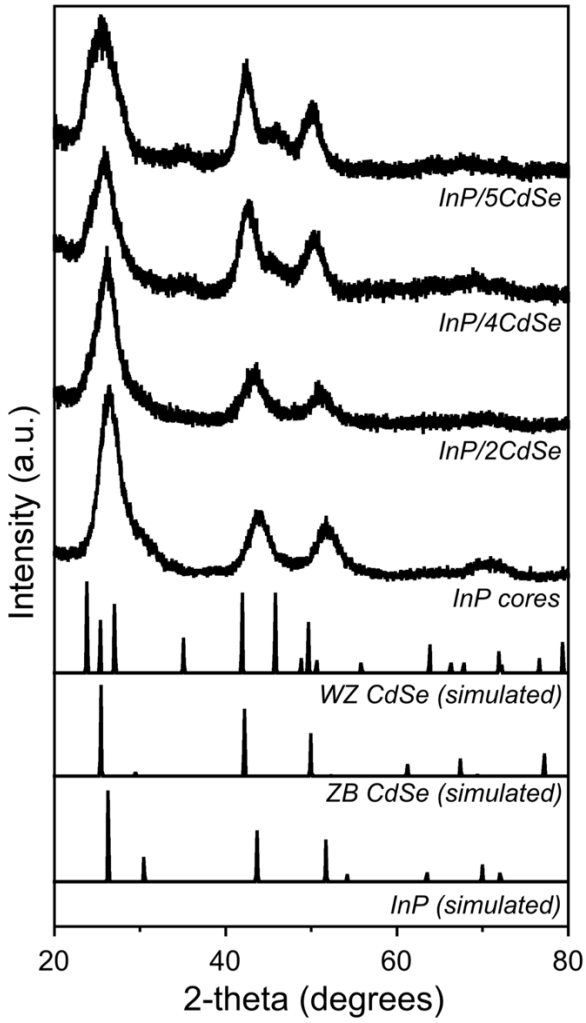

Figure S1. Powder XRD data for InP/CdSe core/shell nanocrystals, along with simulated data for the relevant bulk compounds. The InP cores (~3.5 nm) exhibit a cubic, zinc blende (ZB) crystal structure. At early stages of shell growth (2CdSe), the data suggest that the CdSe shell also adopts a cubic ZB structure. As the CdSe shell is grown thicker, the presence of hexagonal, wurtzite-phase (WZ) CdSe emerges in the diffraction pattern.

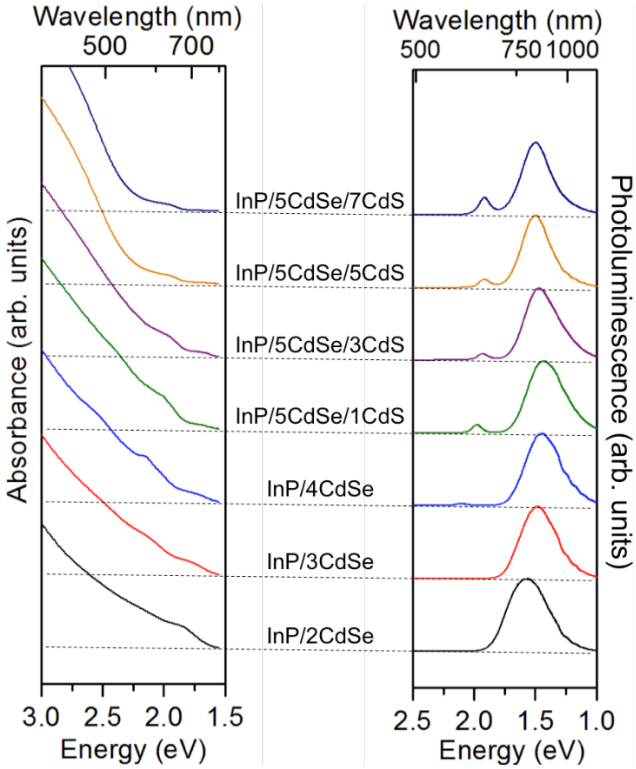

Figure S2. Absorbance and photoluminescence spectra for an InP/CdSe QD shell-thickness series (number indicates approximate number of CdSe shell monolayers; InP core diameter is 3.5 nm), including addition of CdS shells onto InP/5CdSe. A clear CdSe absorption 1S appears for InP/4CdSe, as does a noticeable CdSe visible-PL peak. Note: visible PL here is relatively weak in part because this sample was washed (excess ligands removed) prior to the PL spectrum being obtained.

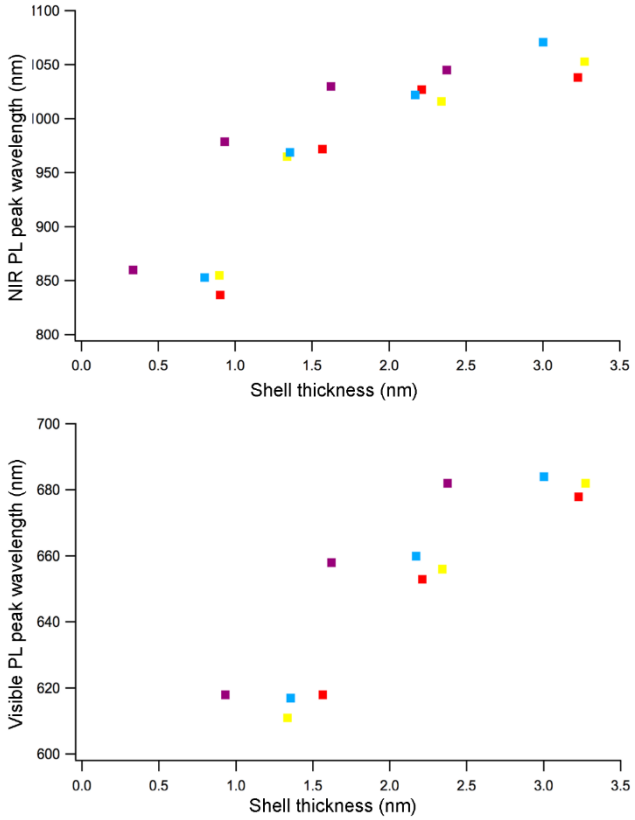

Figure S3. NIR and visible PL peak wavelengths as a function of CdSe shell thickness for an InP/CdSe core-size (InP diameter – red: 1.8 nm, yellow: 1.9 nm, blue: 2.4 nm, purple: 3.3 nm) and shell-thickness (as shown) series.

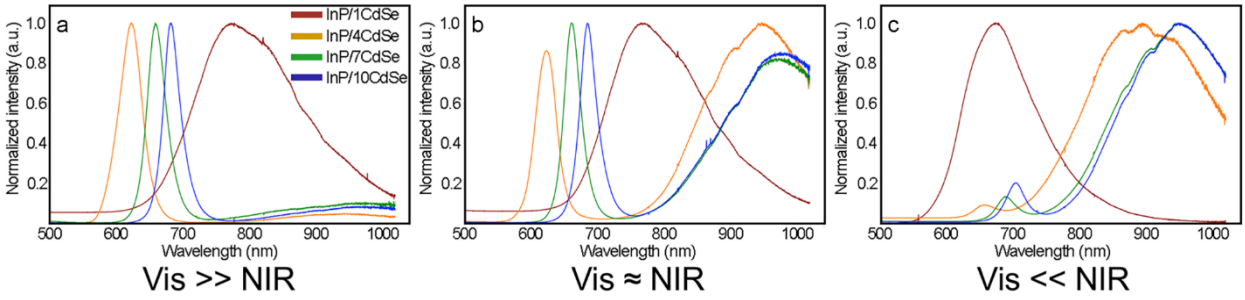

Figure S4. Relative contributions from visible and NIR PL depend on treatment of InP cores prior to shell growth. (a) Visible PL dominates when cores are worked up in air; (b) visible and NIR PL intensities are similar for imperfect air-free work-up, and (c) NIR PL dominates when cores are not removed from their growth solution prior to initiation of shell growth, but visible PL is still present most likely as a result of choice of reactant (In(III) acetate compared to $InCl_3$; see main text).

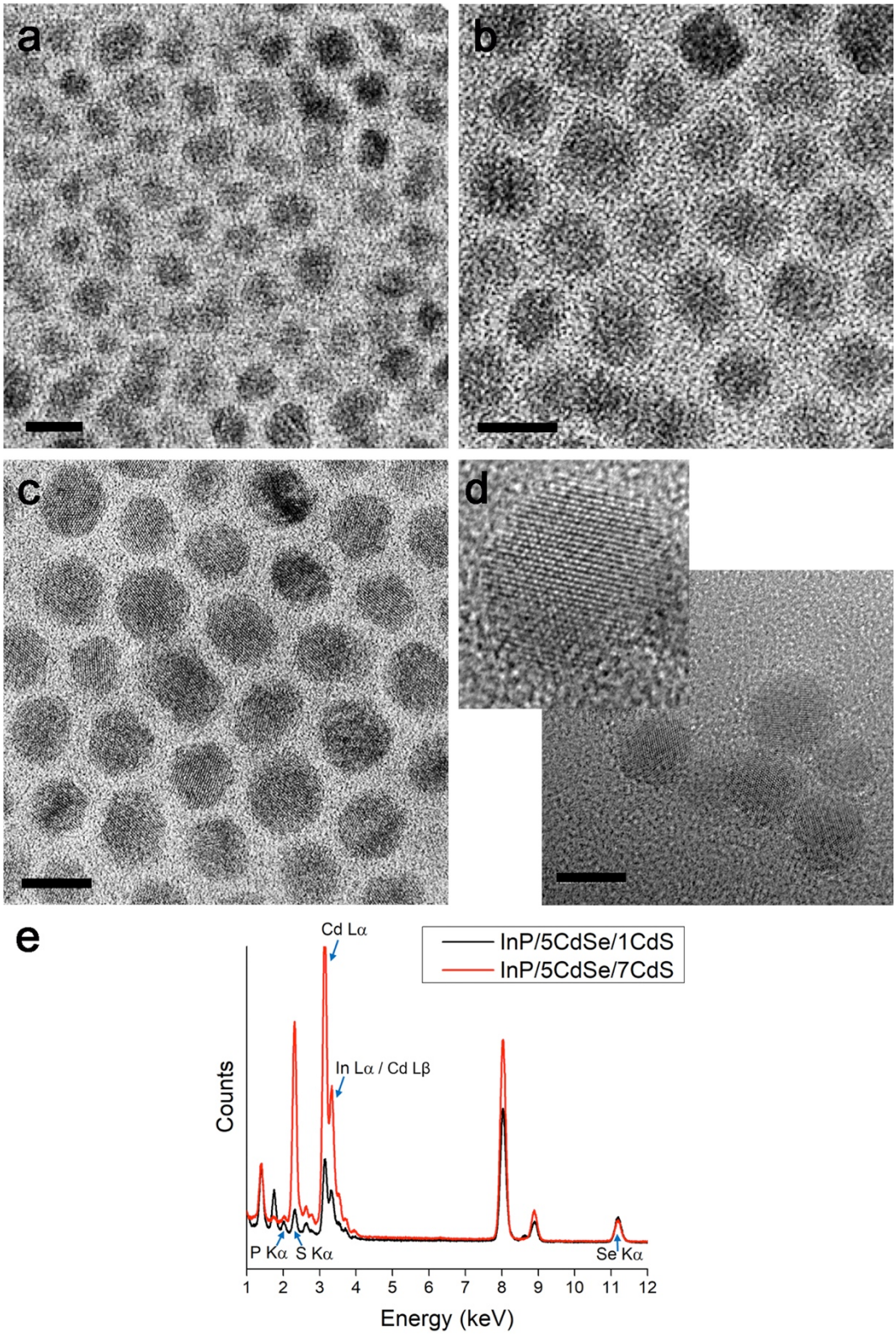

Figure S5. TEM and HR-TEM images of InP/5CdSe/1CdS (7.2 +/- 0.8 nm;), InP/5CdSe/3CdS (9.2 +/- 1.0 nm), (c) InP/5CdSe/5CdS (9.7 +/- 1.2 nm), and (d) InP/5CdSe/7CdS QDs. (e) Energy dispersive X-ray spectroscopy (EDS) data for InP/5CdSe/1CdS and 7CdS; experiments were performed on an FEI Tecnai F30 HRTEM equipped with an EDAX EDS detector. All size determinations based on ~200 particles; scale bar = 10 nm.

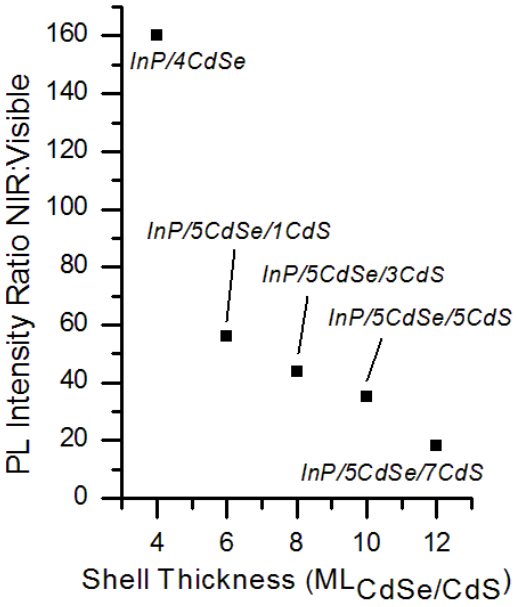

Figure S6. Plot of the ratio of integrated areas under the NIR emission peak to the visible emission peak for each shell thickness that exhibits dual emission. All samples are purified using similar procedures, but the purification of InP/4CdSe (or InP/5CdSe) results in dramatic decrease in visible PL intensity. Addition of CdS shells causes the visible emission peak to be more resilient to washing and removal of excess surface ligands.

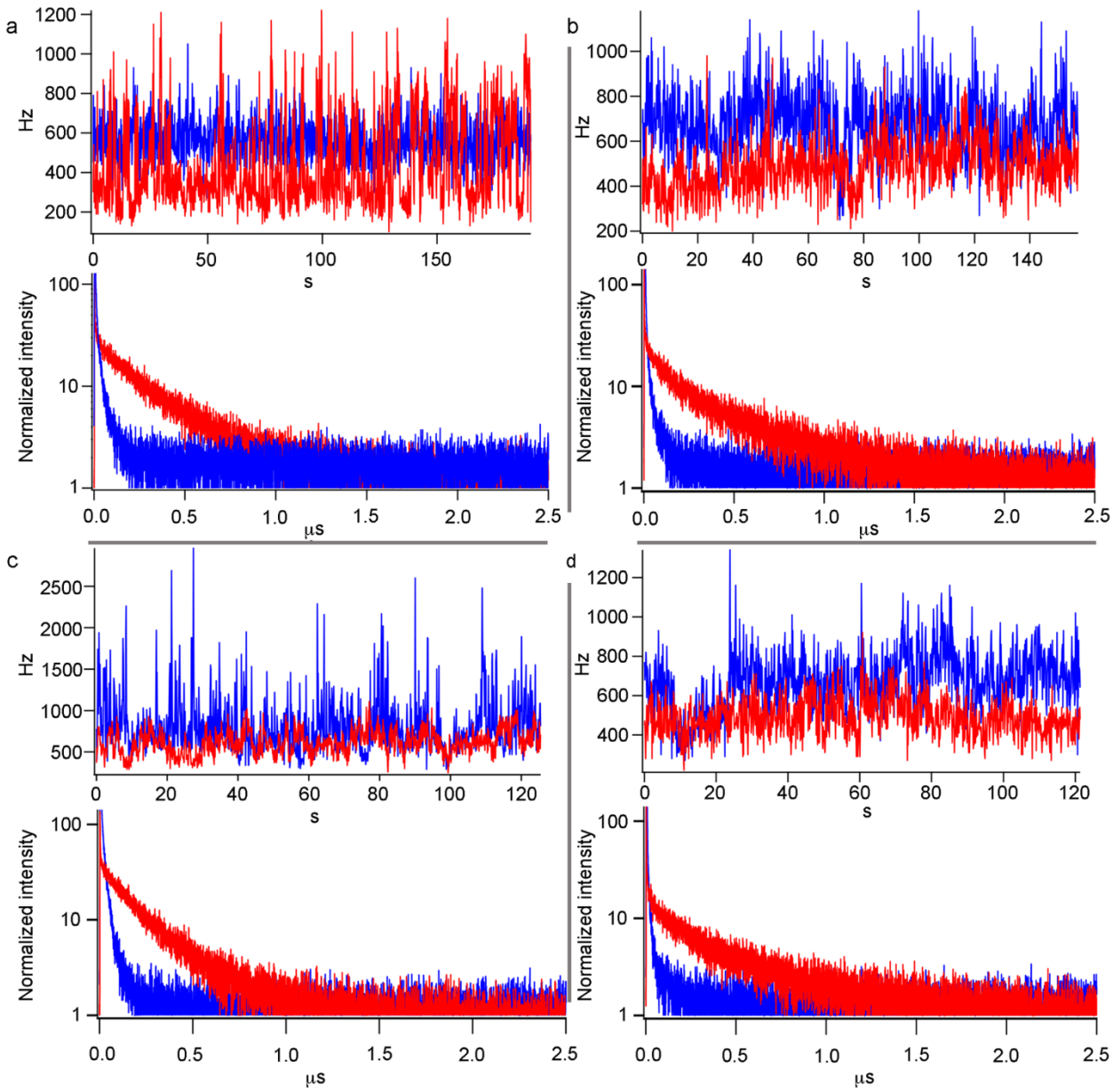

Figure S7. Visible (blue) and infrared (red) simultaneous PL intensity versus time traces and PL decay curves for four InP/CdSe/7CdS gQDs (a-d) (Note: color scheme is opposite that in Figure S8).

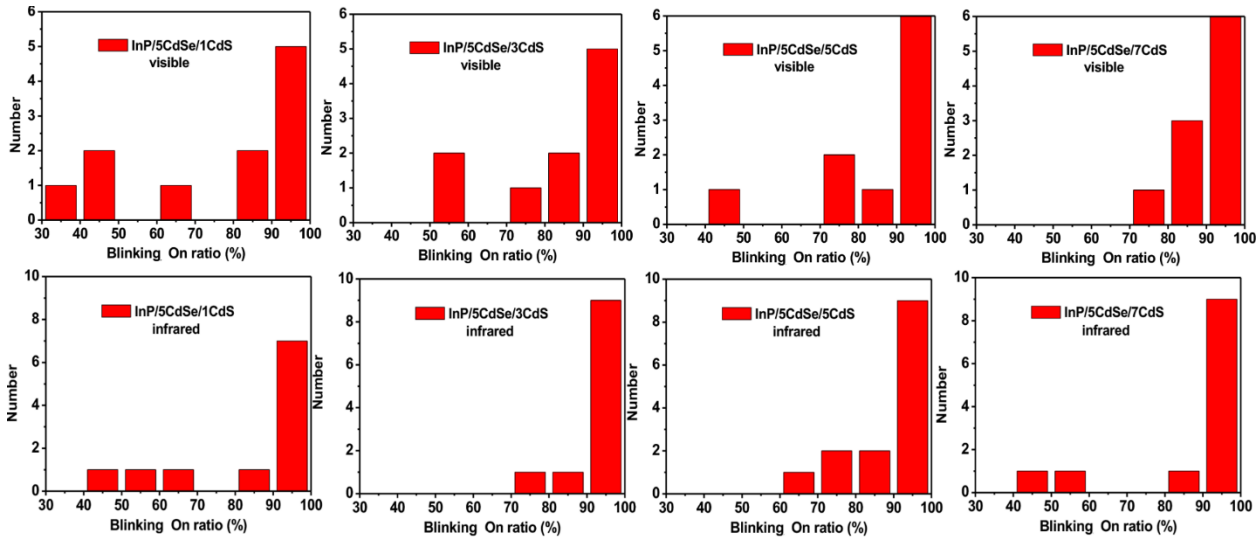

Figure S8. Blinking statistics for InP/5CdSe/1-7CdS shell series for visible (top) and NIR (bottom) emissions. Blinking on-ratio of 95% is considered "non-blinking." From left to right, the percentage of QDs exhibiting dual emission is 76%, 83%, 85%, and 90%.

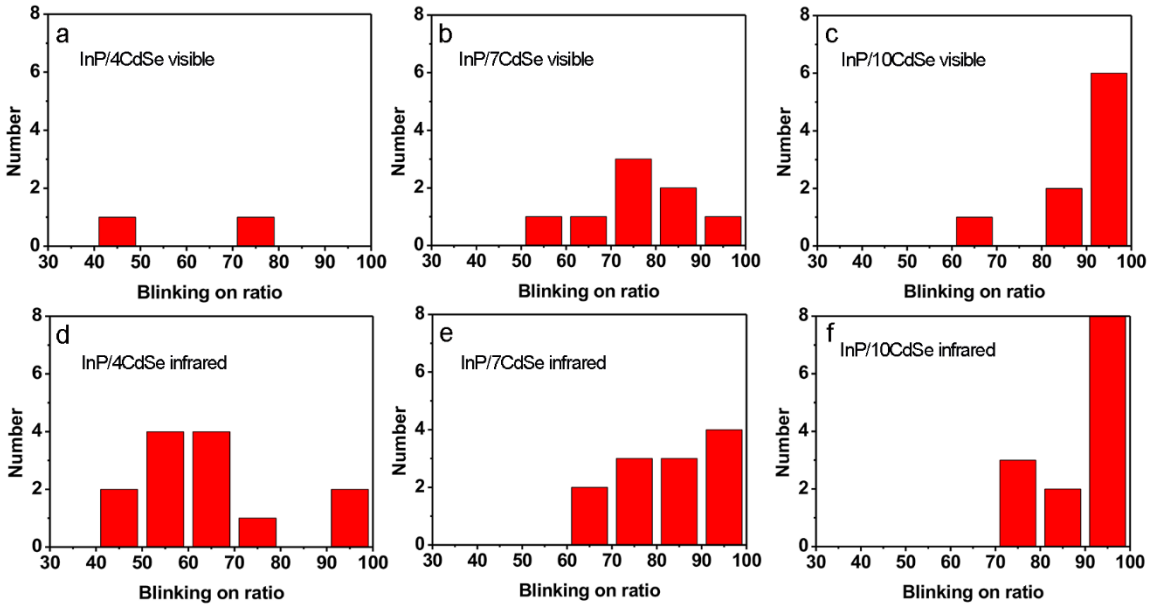

Figure S9 Blinking statistics for InP/CdSe shell series for visible (top) and NIR (bottom) emissions. Again, blinking on-ratio of 95% is considered "non-blinking." Comparing (a) with (d), it is evident that while a total of 13 QDs emitted in the infrared spectral range, only 2 of these QDs also exhibited visible emission. From left to right, the percentage of QDs exhibiting dual emission is 15%, 67%, and 69%.

.

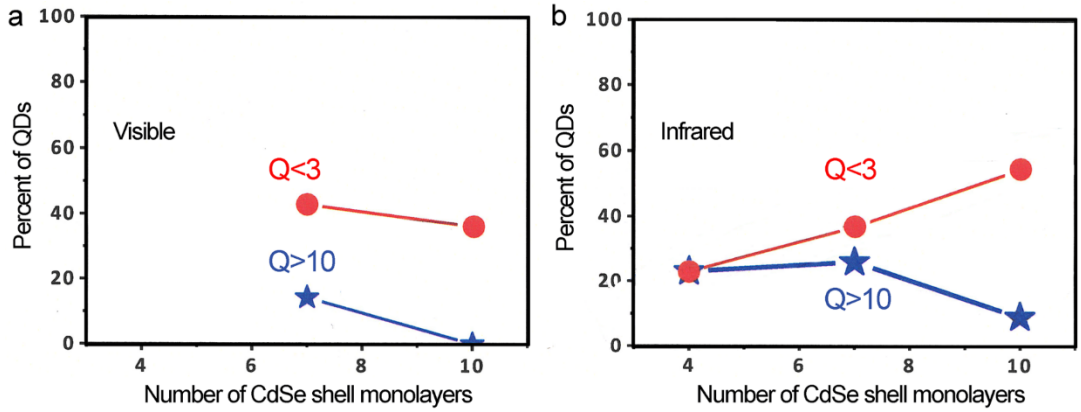

Figure S10. InP/CdSe Mandel Q parameters as a function of number of CdSe monolayers (MLs) for (a) visible and (b) infrared emissions.

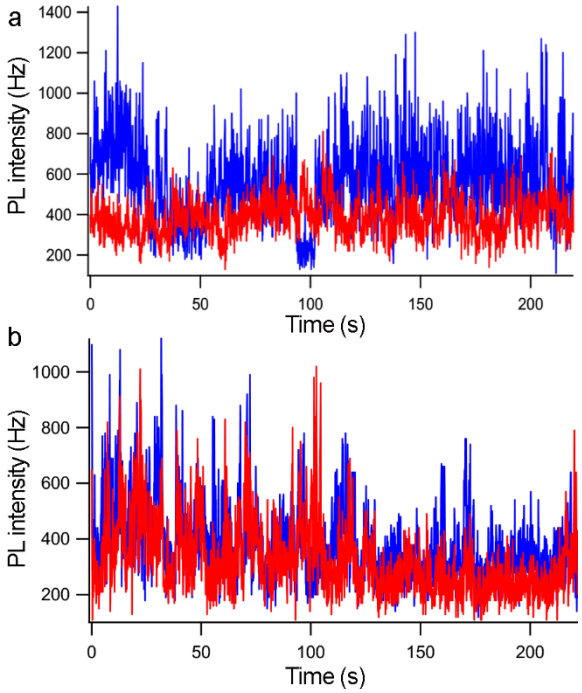

Figure S11. Visible (red) and infrared (blue) simultaneous PL intensity versus time traces for (a) an InP/5CdSe/5CdS gQD and (b) an InP/10CdSe gQD. Both are characterized by blinking on-time percentages of >90% in visible emission, but only the InP/5CdSe/5CdS has a low Mandel Q parameter due to it minimal "flickering," or intensity fluctuation.

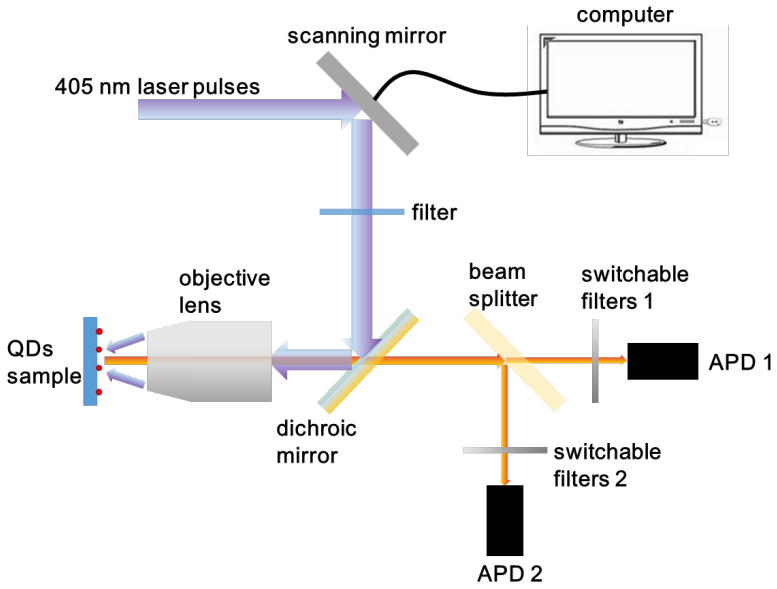

Figure S12. Schematic showing optical setup (simplified for clarity) used for single-nanocrystal optical measurements.